Surface and Coatings Technology, Volume 204, Issues 9–10, 25 January 2010, Pages 1395–1404

Characterization and solderability of cold sprayed Sn-Cu coatings on Al and Cu substrates

J.F. Li, P.A. Agyakwa, C.M. Johnson

School of Electrical and Electronic Engineering, The University of Nottingham, University Park, Nottingham NG7 2RD, United Kingdom

D. Zhang, T. Hussain, D.G. McCartney

School of Mechanical, Materials and Manufacturing Engineering, The University of Nottingham, University Park, Nottingham NG7 2RD, United Kingdom.

Abstract

Cold sprayed Sn coatings approximately of 40 and 25 μm in average thickness were deposited on aluminium and direct bonded copper (DBC) substrates, respectively. Both statistical analysis of coating thickness and roughness analysis of coating/substrate interface and coating surface for the as-sprayed coatings were carried out based on scanning electron microscopy images. The results obtained can be related to substrate types and spraying conditions. Tin oxide on the surfaces of the as-sprayed coatings was revealed by employing X-ray photoelectron spectroscopy analyses and transmission electron microscopy. It came from an oxide shell around feedstock powder particles and was only locally broken down during cold spraying. Although the oxide inhibited fluxless soldering, flux-supported reflow of cold sprayed Sn on the DBC substrate produced Cu/Sn/Cu solder joints that were acceptable for application in electronic packaging and interconnects. In general, measures which can avoid or remove the tin oxide are needed to achieve improved solder joints using cold sprayed Sn coatings as the solder layers.

Keywords: [B] Roughness; [B] Photoelectron spectroscopy; [B] Transmission electron microscopy (TEM); [D] Tin; [D] Tin oxide; [X] [C] Cold spraying

1. Introduction

Cold spray was developed in the mid 1980s at the Institute of Theoretical and Applied Mechanics of the Siberian Division of the Russian Academy of Science in Novosibirsk [1,2]. During cold spraying, powders of ductile metals, usually in the size range of 1 to 50 μm, are accelerated through a de Laval type of nozzle, by a supersonic gas flow, to speeds of 300 to 1200 m/s to impact the substrate or previously deposited powder particles to form a coating. Heated air or nitrogen may be used as the processing gas, but the best quality of coatings is generally achieved by using helium [2-3]. Al and Cu coatings have been the most extensively investigated in cold spray. Studies have included optimization of the spraying process, bonding mechanism, microstructure formation and heat treatment or thermal stability of the deposited coatings [3-9]. A number of other coatings have also been reported to be successfully deposited using cold spray, including Sn, Al-Sn and Cu-Sn coatings as examples [10-14].

Cold sprayed coatings are believed to have relatively low porosity and low content of oxygen [14,15]. As a result, cold spray has been investigated as a method to produce solderable surfaces on materials with poor wettability (e.g. heat sinks, such as Cu on Al) and to deposit brazing and soldering alloys for applications in electronic packaging and interconnects [15,16]. For example, a cold sprayed Cu coating on a heat sink made of Al as a base layer has been successful as a solderable surface for the Sn- or Cu-plated area of electronic devices [15]. In this case, the high kinetic energy of the Cu particles could, on impact, break up the oxide film. For similar electronic applications, cold sprayed Al coatings might also be used as bonding layers, e.g. onto a hard and brittle Al_2O_3 substrate, for depositing other top layers, such as Cu and Sn, using other coating/film process [15].

Another interesting effort in cold spray was the deposition of conducting layers onto plastics [16]. By controlling the spraying process conditions, it was possible to deposit Cu

onto PA 66(nylon 6/6), but the bond strength between the Cu particles and the substrate, as well as between the Cu particles, appeared to be rather low.

Cold spray for depositing Sn-based solder alloy layers has also been investigated although substrate types were not reported [15]. The effects of substrate temperature and gun transverse speed on the formation mechanism of cold sprayed Sn coatings were also systematically investigated by Legoux et al. [11], and a deposition efficiency of less than 5% for Sn coatings on steel substrate was reported. The scanning electron microscopy images of the polished cross sections indicate that a continuous solder layer with a thickness of 20 to 30 μm and a surface roughness, R_a, of 1 – 20 μm could be achieved, see Fig. 13 in [11].

In addition, cold spray was used to deposit Zn-Al-Si brazing alloys for joining Al or Al alloys [17]. In this case, the cold spray process used hot air with temperatures from 100 to 300 °C as the processing gas [18]. The deposited monolith or composite coatings included both brazing materials and corrosion protection materials, which can be used in brazing aluminium fins to plates and tubes of heat exchangers in a single stage.

The purpose of the present work was to assess the potential for employing cold sprayed Sn coatings as solder layers. The main objective of this paper is to systematically characterize the cold sprayed Sn coatings and to clarify the challenges that need to be addressed before cold spray can be reliably used to pre-deposit Sn layers for effective soldering in electronic packaging and interconnects.

Therefore, cold sprayed Sn coatings approximately of 40 and 25 μm in thickness were deposited on aluminium and direct bonded copper (DBC) substrates, respectively. We report here the results including: (i) statistical analysis of thickness and roughness parameters of surface and coating/substrate interface for the as-sprayed coatings based on scanning electron microscopy (SEM) images; (ii) identification of surface oxides on the as-sprayed coatings using X-ray photoelectron spectroscopy (XPS) and transmission electronic microscopy

(TEM); and (iii) results of both flux and fluxless soldering trials intended to join the aluminium and DBC using the cold sprayed Sn coatings as the solder layers.

2. Experimental procedure

2.1 Materials

Pure Sn powder of nominal size range -30 +5 μm mechanically blended with 5wt% of -30 +5 μm pure Cu powder was used as feedstock for cold spray. 5wt% Cu was added into the feedstock because Sn-based solders are generally alloyed with other metals to suppress the well known “tin pest” at temperatures below 13 °C [19]. A SEM image of the blended powders is shown in Fig. 1(a). They have a spherical morphology typical of metallic powders prepared using a gas atomizing process. The corresponding particle size distribution obtained using image analysis method from SEM micrographs is shown in Fig. 1(b), where the powder particles were approximated as ideal spheres and the particle size of 21.3 μm corresponds to the cumulative volume fraction of 0.5.

Cu and Al are used extensively as contact metallizations and/or materials for thermal management in electronic assemblies and systems [20] and were thus selected as materials for the substrates used in these studies. The Al substrate was commercially available 1 mm thick 99.99% Al sheet with a microhardness $Hv_{0.2kg}$ of 35. Prior to cold spraying, it had been cut into 100×12×1 mm coupons. The Cu substrate was direct bonded copper (DBC) that is widely used in power electronics for supporting semiconductor devices. In cross-section, it consists of two layers of 0.3 mm thick Cu (with a microhardness $Hv_{0.2kg}$ of 97) sandwiching a layer of 0.4 mm thick alumina. Before the cold spraying, it had been cut into the coupons of 100×12×1 mm in size. The cut Al and Cu coupons were cleaned using isopropyl alcohol, without the need of any further surface preparation.

2.2 Cold spray

Cold spray was carried out at the University of Nottingham using an in-house constructed cold-gas spraying system, which is described in detail elsewhere [16]. A schematic diagram of the spraying system is shown in Fig. 2, where room temperature helium was employed as the driving gas for both particle acceleration and powder feeding. The powder feedstock was delivered into the gun chamber using a Praxair Model 1264 high pressure powder feeder.

Following initial trials, two sets of processing parameters were employed to spray the feedstock of blended Sn-Cu powder particles. Sample codes and the corresponding processing parameters are listed in Table 1. In all cases, the pressure of the powder carrier gas was 0.1 MPa above that of the main driving gas. All three coatings were produced in a single pass because multiple passes were found to lead to de-bonding of the coatings from the substrates. The stand alone de-bonded coatings produced by two passes were somewhat thicker (100 - 150 μm) than the coatings prepared using a single spraying pass which were typically 25 - 40 μm thick.

2.3 Soldering trials

As presented below, the resulting coating AA2 is discontinuous. Thus only the as-sprayed AA1 and AC1 coatings were cut into pieces of 12×10×1 mm and 15×12×1 mm respectively for soldering experiments. The soldering experiments were carried out using the sample geometries shown in Fig. 3. Because of the deformation of the Al substrate caused during cutting, a layer of 50 μm eutectic Sn-Ag foil was inserted in the middle to improve the gap filling for the AA1 coating. Before the soldering processes, all samples were ultrasonically cleaned using isopropyl alcohol (IPA), rinsed using acetone and deionised water. For purpose of comparison, three reflow processes termed RP1, RP2 and RP3 are listed in Table 2. They were used for both the Al/Sn-SnAg-Sn/Al (AA1) and DBC/Sn-Sn/DBC (AC1) systems.

Of the three reflow processes listed in Table 2, RP1 and RP2 are typical of a fluxless soldering process that might be applied in the assembly of power electronic modules either for die or substrate mount down. Such processes involve the use of solder foil pre-forms typically between 100 and 400 microns in thickness. Forming gas is used to clean the surfaces and vacuum is used to reduce voiding. This process is preferred for making large area (>1cm^2) bonds. Surface abrading used in RP2 is to see whether this could effectively remove surface oxide on the coatings. RP3 is typical of the fluxed solder reflow process that is widely used in electronics assembly. Here a pre-fluxed solder paste is employed and reflow takes place in an air ambient.

After the reflow processes, the interfacial microstructures of the resulting samples were characterized using the same procedures for sample preparation and SEM observation as those used for the as-sprayed Sn coatings and described in the following section.

2.4 Coating characterization by scanning electron microscopy (SEM)

A JEOL 6400 SEM using the secondary electron (SE) signal was used to examine as-sprayed coating top surfaces. To examine coating microstructures in cross-section, the backscattered electron signal (BSE) was employed.

Metallographic cross-sections of the as-sprayed coatings were prepared for thickness and roughness measurement. The coating samples were first cut into pieces approximately 15×5×1 mm and then mounted in epoxy resin that was cured at room temperature for 24 hours. The mounted samples were then successively ground with 400, 800, 1000, 1200 and 2400 grit SiC papers and finally polished using diamond slurries of 3 μm and 1 μm for 10 min and 5 min, respectively.

The image analysis method used to extract the original substrate surface, coating surface and coating/substrate interfacial profiles from the cross-sectional SEM images utilized the Image Processing Toolbox Version 5.0.0 of MATLAB R14SP2 (The Mathworks), and is

schematically shown in Fig. 4. For each sample, three to five images at a resolution of 512×416 pixels and image size of 1175×940 μm were used and the obtained data were merged together. Fig. 4(a) shows a SEM image and Fig. 4(b) reveals the extracted profiles. The thickness of a coating sample can be expressed, in principle, as a function of location x along the coating by:

$$t(x) = z_t(x) - z_b(x), \qquad x \in [0, L_0] \tag{1}$$

where $t(x)$ is the thickness, L_0 is the cross-sectional length of the profiles, $z_t(x)$ and $z_b(x)$ are the vertical coordinates of the profiles of the coating surface and the coating/substrate interface, respectively, see Fig. 4(c). The captured digital SEM images were used to generate data sets and so (1) takes on a discrete form:

$$t_i = z_t(x_i) - z_b(x_i), \qquad i = 1,2,..,n \tag{2}$$

where n is the total number of data points. Then the mean, standard deviation, minimum and maximum values of the thickness data can be calculated as detailed in [21,22]. In addition, the cumulative probability for the resulting thickness data, $f(t_j)$, could be obtained from placing the data in ascending order and letting

$$f(t_j) = \frac{j - 0.5}{n}, \qquad j = 1,2,..,n \tag{3}$$

where j is the jth order in ascending thickness data [21]. If some values of thickness t_j were identical in the ascending order, only the one corresponding to the largest cumulative probability was retained and the others were deleted in the final curve of the cumulative probability curves.

For a surface or interfacial profile (see Fig. 4(c)), the roughness parameters, R_p and R_v are respectively the distances of the highest peak and lowest valley to the central line, and roughness parameter R_a is defined as [23]:

$$R_a = \frac{1}{n}\sum_{i=1}^{n}\left|z(x_i) - \overline{z(x_i)}\right| \tag{4}$$

where $z(x_i)$ $(i=1,2,\ldots,n)$ is the vertical coordinate of the profile as a function of location x_i. The average vertical coordinate:

$$\overline{z(x_i)} = \frac{1}{n}\sum_{i=1}^{n} z(x_i) \tag{5}$$

Here the roughness parameters were calculated from the entire cross-sectional profile extracted from the SEM images, which results in a sampling length shorter than and an accuracy similar to the geometrical product specifications established by the ISO technical committee detailed in [23].

In addition, the intermetallic compounds (IMCs) formed between Sn and Cu after the reflow processes were identified using an Oxford Instruments ISIS energy-dispersive X-ray spectroscopy (EDXS) microanalysis system fitted on the SEM.

2.5 Coating characterization by XPS and TEM

XPS was employed to analyze the chemical state of Sn atoms at the surfaces of the as-received Sn powder particles and the as-sprayed coatings AA1 and AC1. The XPS spectra were collected using the Kratos AXIS ULTRA with a mono-chromated Al Kα X-ray source (1486.6eV) typically operated at 15 mA emission current and 10 kV anode potential. The XPS spectra collected were calibrated using the corresponding C 1s aliphatic peaks. TEM was used to further examine the phases on the coating surface. This was done using a JEOL 2000 FX TEM, fitted with an Oxford Instruments ISIS EDXS microanalysis system. Because of very rough surfaces and brittle nature of the coatings, a few coating particles were obtained using a knife of stainless steel to scratch the surface of coating AC1 and dispersed onto extremely thin carbon film fixed on copper mesh for the TEM analysis.

3. Results

3.1 As-sprayed Sn coatings

3.1.1 Microstructure

Figure 5 presents the SEM images showing the microstructures of the as-sprayed coatings. Despite a few tiny pores, all the three coatings are very dense and their porosity values are lower than 1%. Cu particles are occasionally embedded within the three coatings, with the Cu contents obviously lower than the 5wt% of the feedstock powder (Fig. 5(a) to (c)). The as-sprayed surfaces of the coatings exhibit a cellular morphology of particles that were impacted and bonded on the previously deposited particles (Fig. 5d). However, the flattening of the particles is rather limited.

Using the lower pressure (1.0 MPa) driving helium gas, continuous coatings AA1 and AC1 were achieved on both the Al and Cu substrates. Both the surface and coating/substrate interface profiles are rather rough, and the surface profiles are apparently rougher than the coating/substrate interface profiles (Fig. 5(a) and (c)). Comparing the coatings on the two substrates, the coating AA1 on the Al substrate is thicker, and has a less rough surface but more irregular coating/substrate interface than the coating AC1 on Cu substrate.

Using a higher pressure (2.0 MPa) driving helium gas, the majority of the Sn particles were found to penetrate into the Al substrate more significantly than coating AA1 and the resulting coating AA2 is discontinuous (Fig. 5(b)). The coating/substrate interface became rougher and has similar irregularity to the surface.

No metallurgical interfacial reaction was detected and hence solid state bond has formed between the coatings and the substrates. Craters that were produced due to high-velocity impact of the initial Sn particles had enhanced the bonding of the deformed Sn particles to the substrates and formed the profiles of the coating/substrate interfaces (Fig. 5).

3.1.2 Statistical analysis of coating thickness

The data obtained from the image analysis to based coating thickness measurements were analyzed using the approach described in this section. Fig 6 presents cumulative probability curves of thicknesses variations of the three as-sprayed coatings plotted on normal

probability coordinates, where the vertical axis is in the probability scale representing the inverse of a cumulative Gaussian distribution as expressed as:

$$\Phi^{-1}[F(t)] = -\frac{\mu}{\sigma} + \frac{1}{\sigma}t \tag{7}$$

where μ is the mean, σ is the standard deviation and *F(t)* is the cumulative Gaussian function:

$$F(t) = \frac{1}{\sigma\sqrt{2\pi}} \int_{-\infty}^{t} \exp(\frac{t-\mu}{2\sigma^2})dt \tag{8}$$r

Therefore, for data following an ideal normal distribution, the cumulative probability curve would be a straight line on the normal probability coordinates. As shown in Fig. 6, this is the case for the thickness variations of all the three as-sprayed coatings.

Among the three coatings, a lower slope indicates that the thickness of coating AA2 on Al substrate produced using a higher pressure (2.0 MPa) driving helium gas is more scattered than that of coating AA1 on Al substrate produced using a lower pressure (1.0 MPa) driving helium gas. The coating AC1 on Cu substrate is thinner than, but has uniformity similar to that of coating AA1. The latter can be seen from their cumulative probability curves which are parallel to each other.

The characteristic parameters of the normal distribution, including the mean and standard deviation, together with the minimum and maximum values of the thickness of the three as-sprayed coatings are listed in Table 3. It can be further seen that the average thickness, i.e. the mean of coating AA2 is slightly less than that of coating AA1. All the three coatings have maximum thicknesses that are obviously greater than the diameter of the largest particle in the feedstock powder. In addition, based on the fixed powder feed rate, spraying traverse velocity and step width, the deposition efficiencies of the three coatings were calculated from their average thicknesses listed in Table 3. In this calculation, pores within the coatings were ignored and the density of Sn was taken as 7.287 g/cm^3 for both the powder particles and the coatings. The calculated deposition efficiencies are 46%, 42% and 29% for

the coatings AA1, AA2 and AC1, respectively.

3.1.3 Roughness analysis

The results of roughness measurement for the coating surface, coating/substrate interface and original substrate surface of the three coatings are also listed in Table 3. Compared with the original substrate surfaces, the coating/substrate interfaces are seen to be coarsened with significantly increased roughness parameters. This is because the interfaces consist of craters produced by high-velocity impacting Sn particles during the initial deposition stage. It is thus easily understood that the coating/Al interfaces are more irregular than the coating/Cu interface because the Al substrate is somewhat softer than the Cu substrate. It is interesting to note that the roughness parameters of coating/Al interface are increased with doubling the pressure of driving helium gas.

3.1.4 Surface analysis

XPS spectra can be used to analyze the chemical states of a few layers of atoms at the surface of a material. As shown in Fig. 7, obtained from Sn powder and coating top surfaces, the weak peaks at 484.4 eV for the Sn 3d XPS binding energy correspond to the Sn atoms in the form of metallic tin (Sn^0), while the dominating peaks at 484.4 eV correspond to those of tin oxide (Sn^{4+}) [24]. From the ratio of peak area for Sn^{4+} to that for Sn^0, it can be seen that the surfaces of the as-received Sn powder particles are covered with an oxide shell. This layer of oxide might be formed during the manufacturing process, transportation and storage of the Sn powder. After cold spraying, the oxide shell had just been broken down locally to result in exposure of some fresh Sn atoms on the coating surfaces, as reflected by the increased intensities of the XPS peaks for Sn^0. However, the exposure of fresh Sn atoms is limited and the as-sprayed coating surfaces are still predominately covered by the tin oxide.

Figure 8 gives the TEM results of the particles removed from the top surface of coating AC1. Figs. 8(a) and (d) are TEM images of separate polycrystalline particles. Figs. 8(b) and

(e) are the respective selected area electron diffraction (ED) patterns. The discrete spots on Fig. 8(b) correspond to the interplanar spacings which are consistent with those of SnO_2. The rings drawn on Fig. 8(b) are the patterns which would be produced by a polycrystalline SnO_2 sample. In Fig. 8(e), a number of discrete diffraction spots are visible. Also drawn on Fig. 8(e) are the rings which would be produced by a polycrystalline Sn sample and also a $[\bar{3}3\bar{1}]$ zone axis pattern for Sn. Therefore, the corresponding selected areas in Figs. 8(a) and (d) are SnO_2 and Sn respectively. This is confirmed by the EDXS spectra in Figs. 8(c) and (f), where a more pronounced oxygen peak is seen in Fig. 8(c). Note that the minimum electron beam spot size achievable for the EDXS analysis was approximately 200 nm, and some Cu came from the supporting Cu mesh for the sample. Because of the destructive nature in preparing the TEM sample, it is hard to get the images directly reflecting the distribution of the SnO_2 layer on the coating surface. Nevertheless, from the size of the SnO_2 grains, it can be reasonably deduced that the oxide shell on the as-received Sn powder particles and hence the oxide layer covering most surfaces of the as-sprayed coatings is a few to ten nm in thickness.

3.2 Soldering

3.2.1 Sn coating on Al substrate – coating AA1

After reflow process RP1 under nitrogen, the Sn coating was still mechanically bonded on the Al substrate. However, the coating failed to be joined to the eutectic SnAg solder foil between the substrates (see Fig. 3). The surface of the coating has a profile similar to the as-sprayed surface (Fig. 9(a)). These reflow results indicate that the thin layer of tin oxide on the coating surface is very tenacious. Only a very small part of the molten Sn could have flowed out of the locally fresh surface into the SnAg solder to slightly reduce the average thickness of the coating from 40 to 38 μm.

When the as-sprayed surface of the Sn coating was first manually abraded using grade 4000 SiC paper for 10 seconds, the Sn coating on the two sides of the Al/Sn-SnAg-Sn/Al

sample can be partly joined to the eutectic SnAg solder foil after the reflow process RP2. The effective bonding areas on both sides occupy approximately 40% of the total contact area between the Sn coating and the SnAg solder foil (Fig. 9(b)). Some gaps still remain between the Sn coating and the SnAg solder foil. They are probably associated with the tin oxide left at the valleys of the very rough coating surface after the abrading process.

After the flux reflow process RP3 under air, the Sn coating had de-bonded from the Al substrate (Fig. 9(c)). This can be understood because Al is too active under air. The flux was successful in removing the tin oxide on the Sn coating surface, but it failed to prevent the Al substrate from oxidizing with air to form a thin layer of alumina on its surface. As a result, the gradual spreading of thin alumina along the coating/Al interface has progressively driven the molten Sn away from the Al substrate. Most of the molten Sn coating has moved away and joined into the molten SnAg solder (not visible in Fig. 9(c). A few isolated Sn droplets are attached on the roughened surface of the Al substrate (previously the coating/Al interface).

3.2.2 Sn coating on Cu substrate – coating AC1

After reflow process RP1 under nitrogen, the Sn coatings on the two sides of the DBC/Sn-Sn/DBC sample were not joined together. Again, this can be attributed to tin oxide on the coating surface. Intermetallic compounds (IMCs) Cu_6Sn_5 and/or Cu_3Sn were also found to form between the Sn coating and the Cu substrate (Fig. 10(a)). This reveals that a metallurgical interfacial reaction occurred during the reflow process. Therefore, the oxides on both the Cu substrate and the Sn powder particles were presumably broken down during cold spraying, and the Sn coating has intimate contact with the Cu surface. Unlike the surface profile of the Sn coating on the Al substrate, the surface profile of the Sn coating on the Cu substrate has changed significantly after the reflowing process RP1. This may be related to the modification of flowability of the molten Sn due to the formation of the IMCs at the interface. Otherwise, the surface profile of the thinner Sn coating on the Cu substrate should

be more stable than that of the thicker Sn coating on the Al substrate.

After abrading using SiC paper and then subjected to reflow process RP2, the Sn coatings on the two sides of the DBC/Sn-Sn/DBC sample were locally joined together (Fig. 10(b)). Because the surface of the Sn coating on the Cu substrate is more irregular than the Sn coating on the Al substrate, more tin oxide may remain on the coating surface after the light abrading process. As a result, the ratio of the bonded area to the total contact area was lower than that achieved in the Al/Sn-SnAg-Sn/Al sample under identical abrading and reflow process (Fig. 9(b) and Fig. 10(b)).

By contrast, after the flux reflow process RP3 under air, an effective solder joint was achieved as shown in Fig. 10(c) and (d). Thus, flux is useful to remove the surface tin oxide during the reflow process. The pores and/or voids within the solder joint indicate that further process optimization is required.

For the RP1, RP2 and RP3 samples, the IMC layer between Sn and Cu is approximately 1 μm in thickness. EDXS analysis of the IMC layer quotes a composition of 66 at% Cu and 34 at% Sn (point A in Fig. 10(d)), or 64 at% Cu and 36 at% Sn (point B in Fig. 10(d)). However, because of the effect of beam spreading, this does not reflect the composition of the IMC layer alone. The Cu-Sn IMC could be either Cu_6Sn_5 or Cu_3Sn.

4. Discussion

4.1 Cold spraying

During cold spraying, the bonding is achieved mainly through adiabatic shear instabilities caused by high strain rate deformation due to the high-velocity impact of the powder particles [6]. According to the theoretical investigation in cold spraying process [5,6,11], at least three important velocities are associated with the present Sn coatings. The first one is the critical velocity of a powder particle that must be reached so that the impacting

particle can be bonded on the surface of a substrate. The second one is the critical velocity that is related to the self-bonding capability of the coating material so that a thick coating can be built up. The third one is the erosion velocity above which few coating particles will adhere to the surface of the substrate or previously deposited coating. The three important velocities all decrease with increase in particle size and temperature [5,6]. On the other hand, there also exists a 'critical' particle diameter above which thermal diffusion is sufficiently limited to allow localized shear instability to occur at the surface of an impacting spherical particle [6]. For example, Schmidt et al [6] gave a value of 9 μm for Sn particle under certain assumed characteristic length for thermal diffusion and critical velocity for impact. Actually, the critical velocity for impact is difficult to be predicted and depends on particle size, morphology and thickness of surface oxide layer etc. Nonetheless, a particle whose size is smaller than a similar 'critical' diameter would not reach the extent of shear instability for bonding.

Overall, the impacting velocity of a Sn powder particle increases with increasing pressure of the driving helium gas, and the impacting velocity of a larger Sn particle is slower than that of a smaller Sn particle under an identical pressure of the driving helium gas. For the coatings AA2 formed on the Al substrate using a higher pressure of the driving helium gas, the Sn particles had higher impacting velocities, and thus relatively larger Sn particles had reached the first critical velocity and been bonded on the substrate. These impacting particles would result in deeper and larger craters on the original surface of the substrate. This is the reason why the coating/substrate interface consisting of the craters is more irregular than the coating/substrate interface in the coating AA1 produced using a lower pressure of the driving helium gas. On the other hand, under a higher pressure of the driving helium gas, a few larger Sn particles could have achieved the second critical velocity. It is also more likely for smaller Sn particles to reach the erosion velocity. As a result, the coating AA2 is discontinuous and

has an average thickness slightly smaller than the coating AA1. The roughness parameters are similar to each other for the surfaces of both coatings.

For the coating AC1, on the relatively harder Cu substrate, the largest Sn particle which reached the first critical velocity is smaller than that for the coating AA1. Consequently, fewer and smaller Sn particles could have deposited on the initial surface of the Cu substrate. The average thickness of this coating is thus somewhat lower, and the coating/substrate interface consisting of the impact craters is smoother than the coating AA1. However, the surface of the coating AC1 appears to be more irregular. This may be caused by compensation of the deformation of the Sn particles impacting on the different substrate.

From the above discussion, it can be seen that only Sn particles within a relatively narrow size range can be effectively deposited. Those outside this range, both smaller and larger, would not have been deposited and this explains why the coating thickness variations all follow a normal distribution even though the feedstock powder has a multi-mode distribution. During cold spraying, the coating AA2 suffered stronger erosion whilst also being formed from the deposition of larger Sn particles than the coating AA1 as a result of the higher particle velocities. Thus the thickness variation of the AA2 coating is seen to be more scattered than that of the AA1 coating.

The deposition efficiencies of the Sn coatings achieved in the present work are clearly higher than the maximum deposition efficiency 5% of cold sprayed Sn on steel substrates reported by Legoux et al [11]. This can be attributed to the following two facts. First, Al and Cu substrates were used that are softer than steel. Secondly, a lower pressure of the driving helium gas was used which probably resulted in lower particle velocities than in Ref. [11]. Although the impact velocities were not measured, a certain proportion of the Sn particles must have achieved the impact velocities between the second critical velocity and the erosion velocity. In Legoux et al's investigation [11], the impact velocities of the Sn particles were

thought to be already higher than the erosion velocity. In addition, as aforementioned, a second spray pass led to the de-bonding of the deposited Sn coatings. This could be attributed to the accumulation of residual stress with increasing thickness of the coating. Nevertheless, it should be possible to build thicker Sn coatings using the present spraying conditions if the residual stress can be controlled. On the other hand, the de-bonded coatings produced using two passes were almost four times those produced using single pass. This may be due to the fact that more particles contributed to roughening the substrate surfaces and/or were difficult to deposit on the previously relatively smooth surfaces during the first pass. As also reported by Legoux et al [11], many Sn particles can be deposited on the sandblasted surface, but no was found to bond on the polished surface of a steel substrate.

In Ning et al.'s work on cold sprayed Al-Sn coatings on Al6061, copper and SUS 304 substrates, melting of the tin phase was reported [14]. However, this is not the case for the present Sn coatings deposited on both Al and Cu substrates. If the melting of Sn had occurred, Cu_6Sn_5 intermetallic would have been observed at the coating/Cu interface of the as-sprayed Sn coating AC1. This is because the formation of Cu_6Sn_5 IMC was found to be almost instantaneous once fresh Cu was put in contact with liquid Sn [25].

4.2 Solderability

According to the Al-Sn binary phase diagram, no IMC can be formed between Al and Sn [26]. The mechanical bonding between the cold sprayed Sn coating and the Al substrate was seen to be stable after the reflow process under nitrogen (RP1 and RP2). If the surface oxide on the coating can be avoided or effectively removed, cold sprayed Sn coatings in combination with a reflow process under vacuum and/or inert environment would provide an opportunity to solder Al or Al alloy components together. As presented in the results, the surface oxide came from the as-received Sn powder, rather than produced during the cold spraying process. The use of flux would lead to de-bonding of the sprayed Sn coating from

the Al substrate. Therefore, suitable approaches have to be investigated for effective removal of the surface oxide without damaging the bonding between the coating and the substrate. Possible approaches include plasma cleaning of the sprayed Sn coatings or use of ultrasonic scrubbing during the reflow process to break down the surface oxide.

The problem associated with the surface oxide also existed for the soldering of the Sn coating on the Cu substrate under the fluxless reflow conditions. However, this problem was resolved using the flux-supported reflow process. Given that some pores or voids normally exist in conventional solder joints, the quality of the Cu/Sn/Cu solder joint achieved using the cold sprayed Sn coating as the solder layer under the flux-supported reflow condition has the potential to be acceptable for application in electronic packaging and interconnects. Strong flux may be further investigated to reduce the pores or voids within the solder joints.

Generally speaking, the surface roughness needs to be considerably less than the coating thickness to ensure uniformity of the resulting solder thickness and reduce the possibility of voiding. A rougher surface might also result in poor wetting especially for fluxless processes. The surface roughening of substrate should be also noted when considering cold spraying to deposit Sn layers for soldering in electronic packaging and interconnects. As described by the results of roughness analysis, the surface of any substrate used to deposit the Sn layer must have compatible roughness parameters *Rp* and *Rv,* close to 20 µm for the Al substrate, and close to 10 µm for the Cu substrate (Table 3). They were generally the results of surface activation for the substrate subjected to impact of the feedstock powder particles. The contact metallization layers, e.g. Cu or Ni, on semiconductor device are generally thinner than 5 µm. With this consideration, the Sn coatings can be deposited on the supporting substrate, base-plate of heat sink, but not on the semiconductor devices. In addition, it should be possible to reduce the surface roughness of the substrate to some extent by using a finer particle size.

5. Conclusions

Sn powder has been successfully deposited by a single cold spray pass on pure Al and DBC substrates.

The coating/substrate interface roughness depended on the substrate type, but the coating surface roughness is relatively insensitive.

SnO_2 was found on the surface of feedstock powder and also on the surfaces of cold sprayed coatings.

Under reflow process condition RP1, no solder bond did form with either Al or DBC substrate samples.

With identical procedure but following surface abrading, bonding was improved: with Al substrate bonding increased with a Sn-Ag solder interlayer, and with DBC substrate the discrete boding between cold sprayed layers was observed.

Effective solder joint with a flux enhanced reflow process is achieved with the DBC substrate, but not with the Al substrate.

In the case of DBC, IMCs formed during soldering trials, showing a metallurgically clear Sn/Cu interface.

Acknowledgements

This research was funded by the Engineering and Physical Science Research Council and the Innovative Electronic Manufacturing Research Centre in the UK.

References

[1] A.P. Alkhimov, V.F. Kosarev, A.N. Papyrin, Sov. Phys. Dokl. 35 (1990) 1047.

[2] R.C. Dykhuizen, M.F. Smith, J. Therm. Spray Technol. 7(2) (1998) 205.

[3] T. Stoltenhoff, H. Kreye, H.J. Richter, J. Therm. Spray Technol. 11(4) (2002) 542.

[4] D. Zhang, P.H. Shipway, D.G McCartney, J. Therm. Spray Technol. 14(1) (2005) 109.

[5] T. Schmidt, F. Gaertner, H. Kreye, J. Therm. Spray Technol. 15(4) (2006) 488.

[6] T. Schmidt, F. Gartner, H. Assadi, H. Kreye, Acta Mater. 54 (2006) 729.

[7] F. Gaertner, T. Schmidt, H. Kreye, Mater. Sci. Forum 534-536 (2007) 433.

[8] M. Fukumoto, H. Wada, K. Tanabe, M. Yamada, E. Yamaguchi, A. Niwa, M. Sugimoto, M. Izawa, J. Therm. Spray Technol. 16(5-6) (2007), 643.

[9] P.S. Phani, D.S. Rao, S.V. Joshi, G. Sundararajan, J. Therm. Spray Technol. 16(3) (2007) 425.

[10] J. Vlcek, L. Gimeno, H. Huber, E. Lugscheider, J. Therm. Spray Technol. 14(1) (2005) 125.

[11] J.G. Legoux, E. Irissou, C. Moreau, J. Therm. Spray Technol. 16(5-6) (2007) 619.

[12] W.Y. Li, C.J. Li, H. Liao, C. Coddet, Appl. Surf. Sci. 253(14) (2007) 5967.

[13] X. Guo, G. Zhang, W.Y. Li, L. Dembinski, Y. Gao, H. Liao, C. Coddet, Appl. Surf. Sci. 254(5) (2007) 1482.

[14] X.J. Ning, J.H. Jang, H.J. Kim, C.J. Li, C. Lee, Surf. Coat. Technol. 202(9) (2008) 1681.

[15] S. Marx, A. Paul, A. Koehler, G. Huettl, J. Therm. Spray Technol. 15(2) (2006) 177.

[16] E. Calla, Cold Gas Spraying of Copper and Tin onto Metallic and Non Metallic Substrates, Ph. D. Thesis of the University of Nottingham (2005).

[17] B.A. Gillispie, Z. Zhao, J. Robert, H. Van Thomas, Y. Luo, H.F. Hutchins, Product and method of brazing using kinetic - sprayed coatings, US Patent 6 949 300 B2 (2005).

[18] T.H. Van Steenkiste, J.R. Smith, R.E. Teets, J.J. Moleski, D.W. Gorkiewicz, R.P. Tison, D.R. Marantz, K.A. Kowalsky, W.L. Riggs, P.H. Zajchowski, B. Pilsner, R.C. McCune, K.J. Barnett, Surf. Coat. Technol. 111(1) (1999) 62.

[19] G. Humpston, D.M. Jacobson, Principles of Soldering, ASM International, Materials Park, Ohio 44073-0002, 2004.

[20] D.D.L. Chung, Appl. Therm. Eng. 21 (2001) 1593.

[21] C.K. Lin, C.C. Berndt, J Mater. Sci 30 (1995)111.

[22] J.F. Li, C.X. Ding, J Mater. Sci. Lett. 18 (1999) 1591.

[23] S. Guessasma, G. Montavon, C. Coddet, Surf. Coat. Technol. 173 (2003) 24.

[24] W.K. Choi, J.S. Cho, S.K. Song, H.J. Jung, S.K. Koh, Jpn. J. Appl. Phys. 35 (1996) 5820.

[25] T. Laurila, V. Vuorinen, J.K. Kivilahti, Mater. Sci. Eng. R. 49 (2005) 1.

[26] Al-Sn phase diagram, http://www.crct.polymtl.ca/FACT/phase_diagram.php?file=Al – Sn.jpg&dir=SGTE.

Captions of tables

Table 1 Sample codes and the main processing parameters of the cold sprayed Sn-Cu coatings

Table 2 Reflow parameters of the three soldering trials

Table 3 Results of thickness measurement and surface roughness analysis of the as-sprayed Sn coatings

Captions of Figures

Fig. 1 (a) SEM image and (b) cumulative particle size of the mechanically blended 95wt% Sn plus 5wt% Cu powder feedstock.

Fig. 2 Schematic diagram of the cold spray system.

Fig. 3 Schematic sample geometries for the soldering experiments: (a) Al/Sn-SnAg-Sn/Al (AA1) and (b) DBC/Sn-Sn/DBC (AC1) systems.

Fig. 4 Schematic illustration to calculate the roughness parameter and fractal dimensions from an original cross-sectional SEM image: (a) SEM image taken from the as-sprayed coating AA1; (b) the extracted profiles of both the coating surface and the coating/substrate interface; and (c) the roughness parameters R_p and R_v and the quantities used to calculate the roughness parameter R_a.

Fig. 5 SEM images of the three as-sprayed Sn coatings: (a) AA1, polished cross section; (b) AA2, polished cross section; (c) AC1, polished cross section; and (d) AC1, as-sprayed surface.

Fig. 6 Cumulative probability curves of the thickness variations of the three as-sprayed coatings on normal probability coordinates.

Fig. 7 Sn 3d XPS spectra for the as-received Sn powder and the as-sprayed coatings AA1 and AC1. A_{Sn}^{4+} and A_{Sn}^{0} represent the areas of the peaks corresponding to Sn^{4+} and Sn^{0} states.

Fig. 8 TEM results of particles removed from the surface of coating AC1: (a) TEM image of one Sn particle; (b) selected area ED spots distributed along the diffraction rings drawn for

SnO_2; (c) EDXS spectrum showing relatively higher O content around the selected area; (d) TEM image of another Sn particle; (e) selected area ED spots of zone $[\bar{3}3\bar{1}]$ or distributed along the diffraction rings drawn for Sn; and (f) EDXS spectrum showing low O content around this selected area.

Fig. 9 SEM images of the polished cross sections of the Al/Sn-SnAg-Sn/Al (AA1) samples following different reflow processes: (a) RP1; (b) RP2; and (c) RP3.

Fig. 10 SEM images of the polished cross sections of the DBC/Sn-Sn/DBC (AC1) samples following different reflow processes: (a) RP1; (b) RP2; (c) RP3, and (d) also RP3, enlargement view showing the morphology of intermetallic layer.

Table 1 Sample codes and the main processing parameters of the cold sprayed Sn-Cu coatings

Sample code	AA1	AA2	AC1
Substrate	Al	Al	DBC
He pressure (MPa)	1.0	2.0	1.0
Powder feed rate (g/min)	15	15	15
Stand off distance (mm)	20	20	20
Gun traverse speed (mm/s)	100	100	100

Table 2 Reflow parameters of the three soldering trials

Soldering trial	Surface preparation	Reflow temperature and environment profiles
RP1	None	1. Pre-heated up to 200 °C and evacuated below 5 mbar for 3 minutes; 2. Held at 200 °C and purged with 2%$H_2$98%N_2 forming gas (450 L/h at 1.5 bar) for 10 minutes; 3. Heated up to 260 °C and evacuated below 5 mbar for 3 minutes; 4. Held at 260 °C under nitrogen flow of 450 L/h at 1.5 bar for 5 minutes; 5. Cooled down to room temperature within 5 minutes.
RP2	As-sprayed surfaces of the Sn coatings were manually abraded using grade 4000 SiC paper for 10 seconds	Identical to those above for soldering trial RP1.
RP3	As-sprayed surfaces of the Sn coatings were covered with a layer of mild active resin flux	1. Pre-heated up to 200 °C under air for 3 minutes; 2. Further heated up to 260 °C under air over 2 minutes; 3. Held at 260 °C under air for 5 minutes; 4. Cooled down to room temperature naturally.

Table 3 Results of thickness measurement and surface roughness analysis of the as-sprayed Sn coatings

Sample code		AA1	AA2	AC1
Coating thickness	*Mean* (μm)	39.7	35.7	25.1
	Std Dev (μm)	7.8	11.4	9.1
	t_{min} (μm)	16.1	0.0	4.6
	t_{max} (μm)	64.5	69.8	48.8
Coating surface	R_a (μm)	5.2	5.7	6.9
	R_p (μm)	23.8	21.9	24.5
	R_v (μm)	20.1	15.4	17.5
Coating/substrate interface	R_a (μm)	4.9	6.3	2.6
	R_p (μm)	18.1	20.1	8.0
	R_v (μm)	15.6	21.8	9.6
Original substrate surface	R_a (μm)	2.3	2.3	1.3
	R_p (μm)	7.8	7.8	3.6
	R_v (μm)	9.1	9.1	2.9

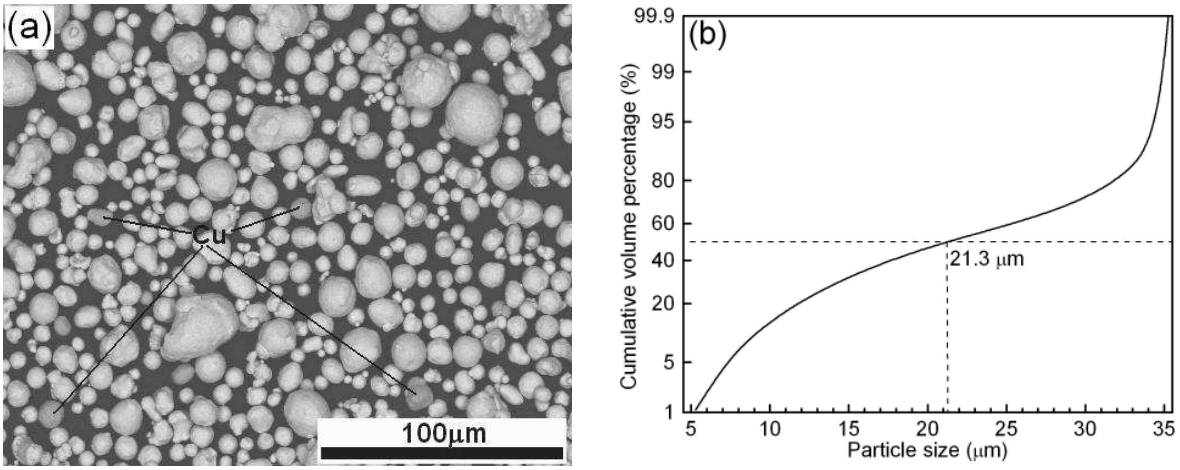

Fig. 1 (a) SEM image and (b) cumulative particle size of the mechanically blended 95wt% Sn plus 5wt% Cu powder feedstock.

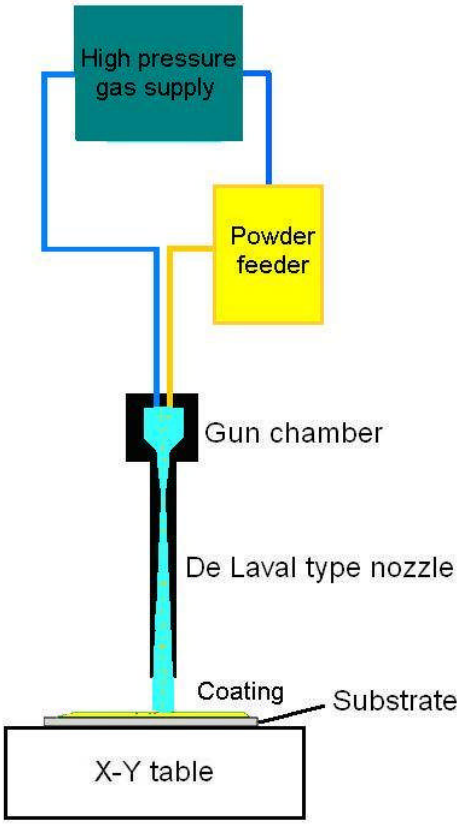

Fig. 2 Schematic diagram of the cold spray system.

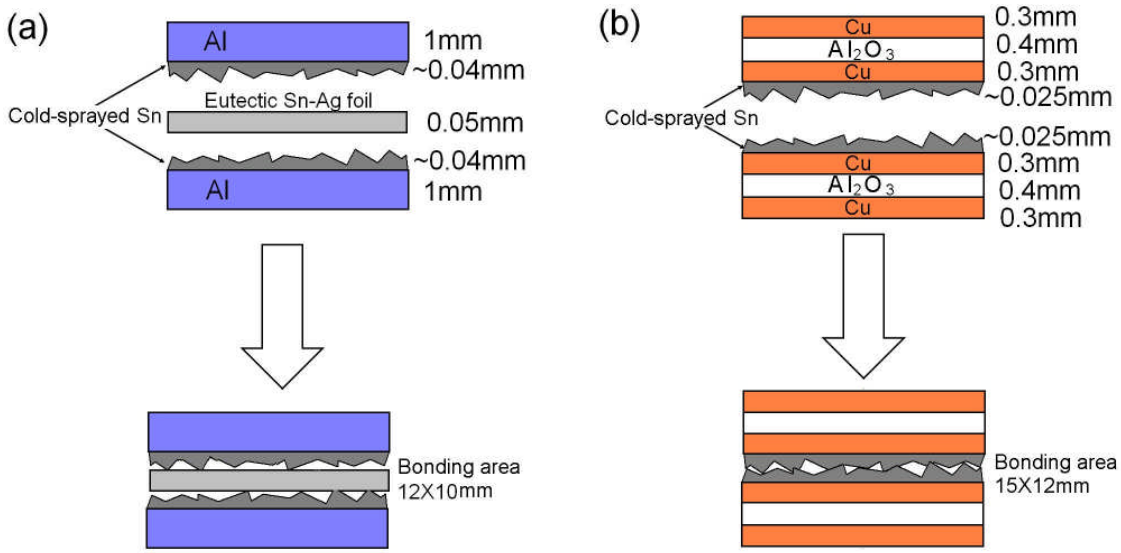

Fig. 3 Schematic sample geometries for the soldering experiments: (a) Al/Sn-SnAg-Sn/Al (AA1) and (b) DBC/Sn-Sn/DBC (AC1) systems.

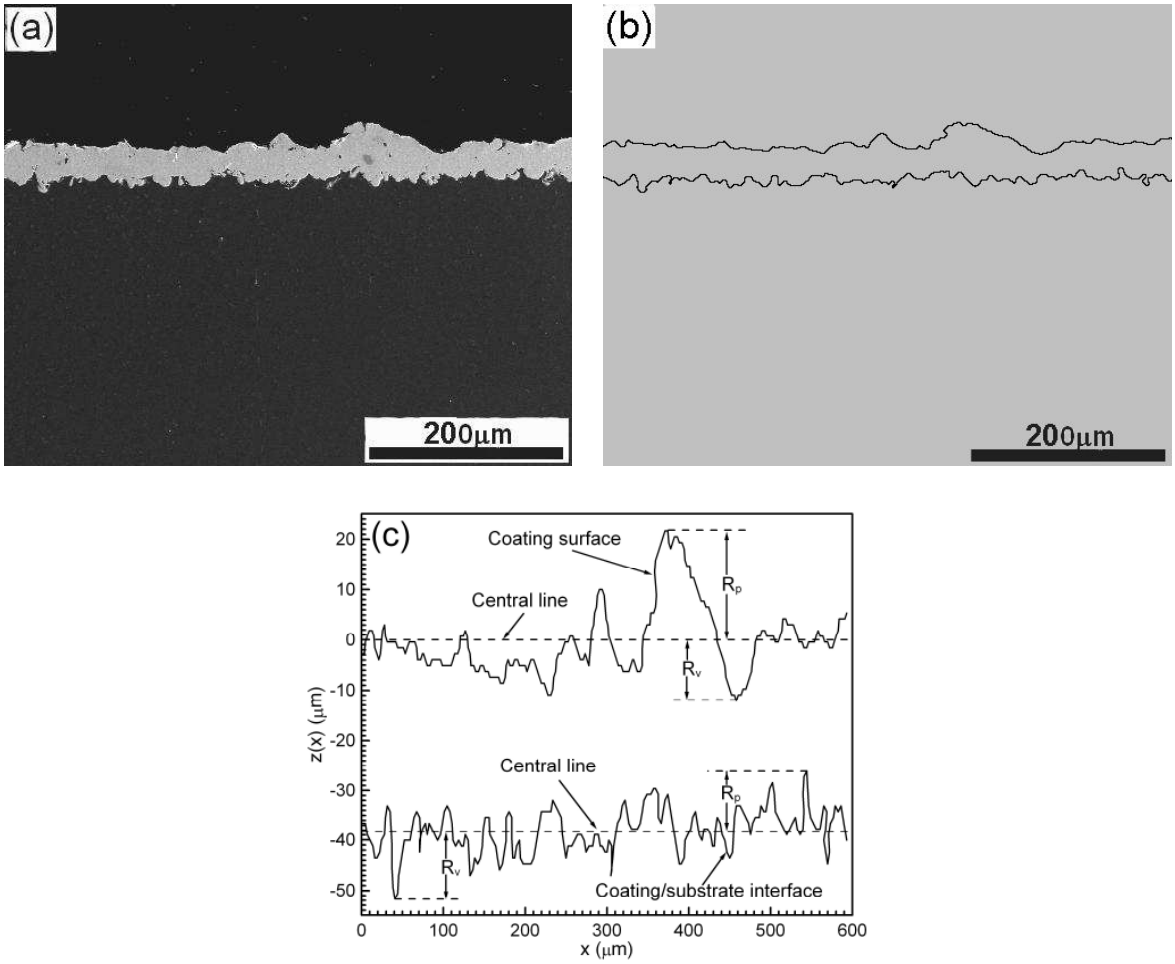

Fig. 4 Schematic illustration to calculate the roughness parameter and fractal dimensions from an original cross-sectional SEM image: (a) SEM image taken from the as-sprayed coating AA1; (b) the extracted profiles of both the coating surface and the coating/substrate interface; and (c) the roughness parameters R_p and R_v and the quantities used to calculate the roughness parameter R_a.

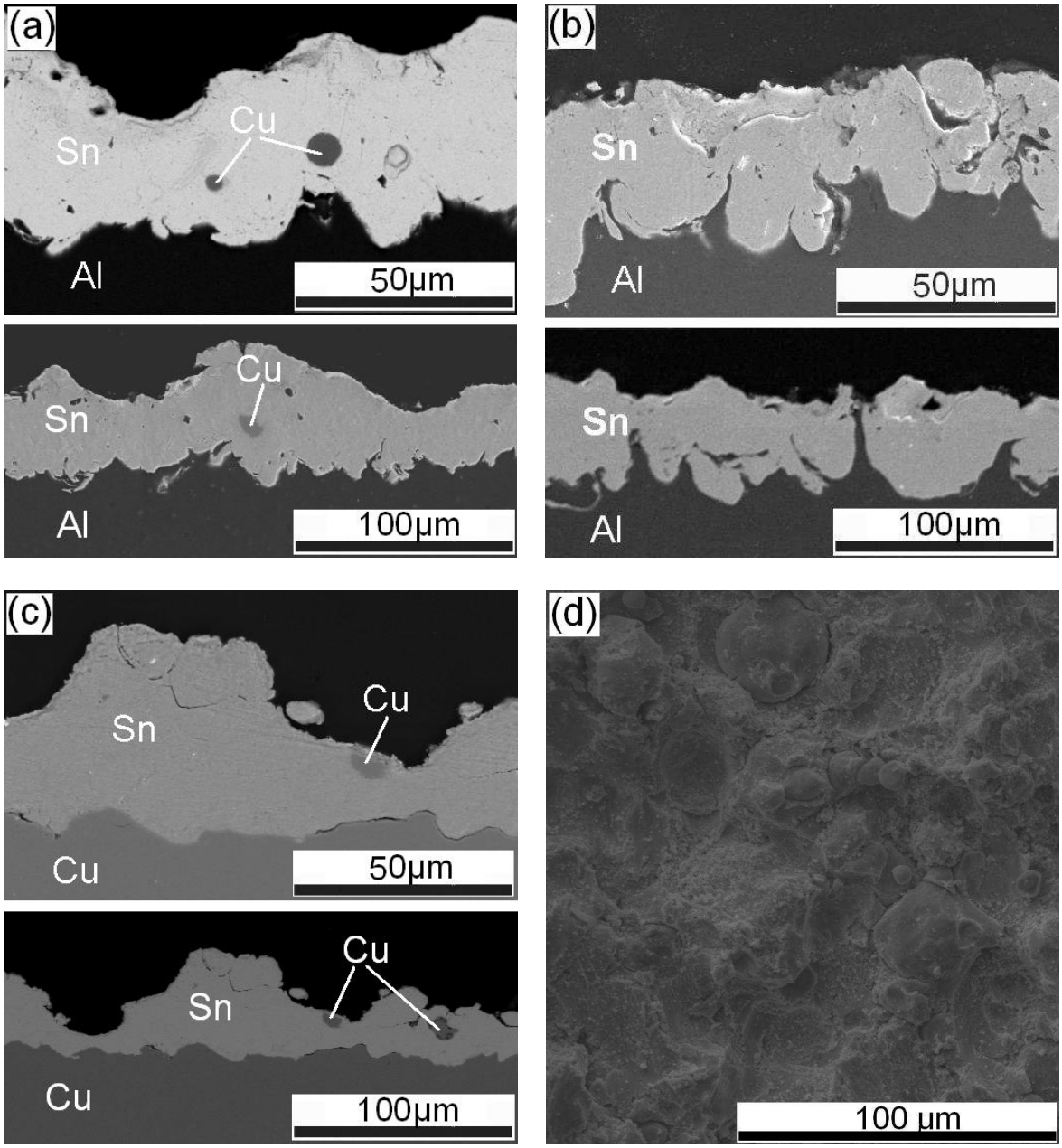

Fig. 5 SEM images of the three as-sprayed Sn coatings: (a) AA1, polished cross section; (b) AA2, polished cross section; (c) AC1, polished cross section; and (d) AC1, as-sprayed surface.

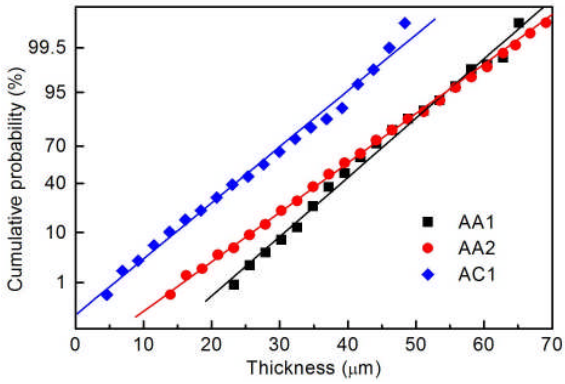

Fig. 6 Cumulative probability curves of the thickness variations of the three as-sprayed coatings on normal probability coordinates.

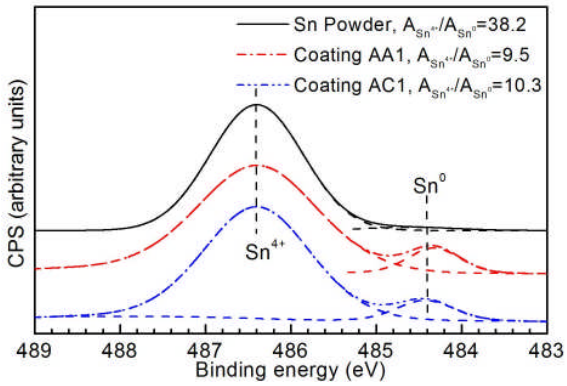

Fig. 7 Sn 3d XPS spectra for the as-received Sn powder and the as-sprayed coatings AA1 and AC1. A_{Sn}^{4+} and A_{Sn}^{0} represent the areas of the peaks corresponding to Sn^{4+} and Sn^{0} states.

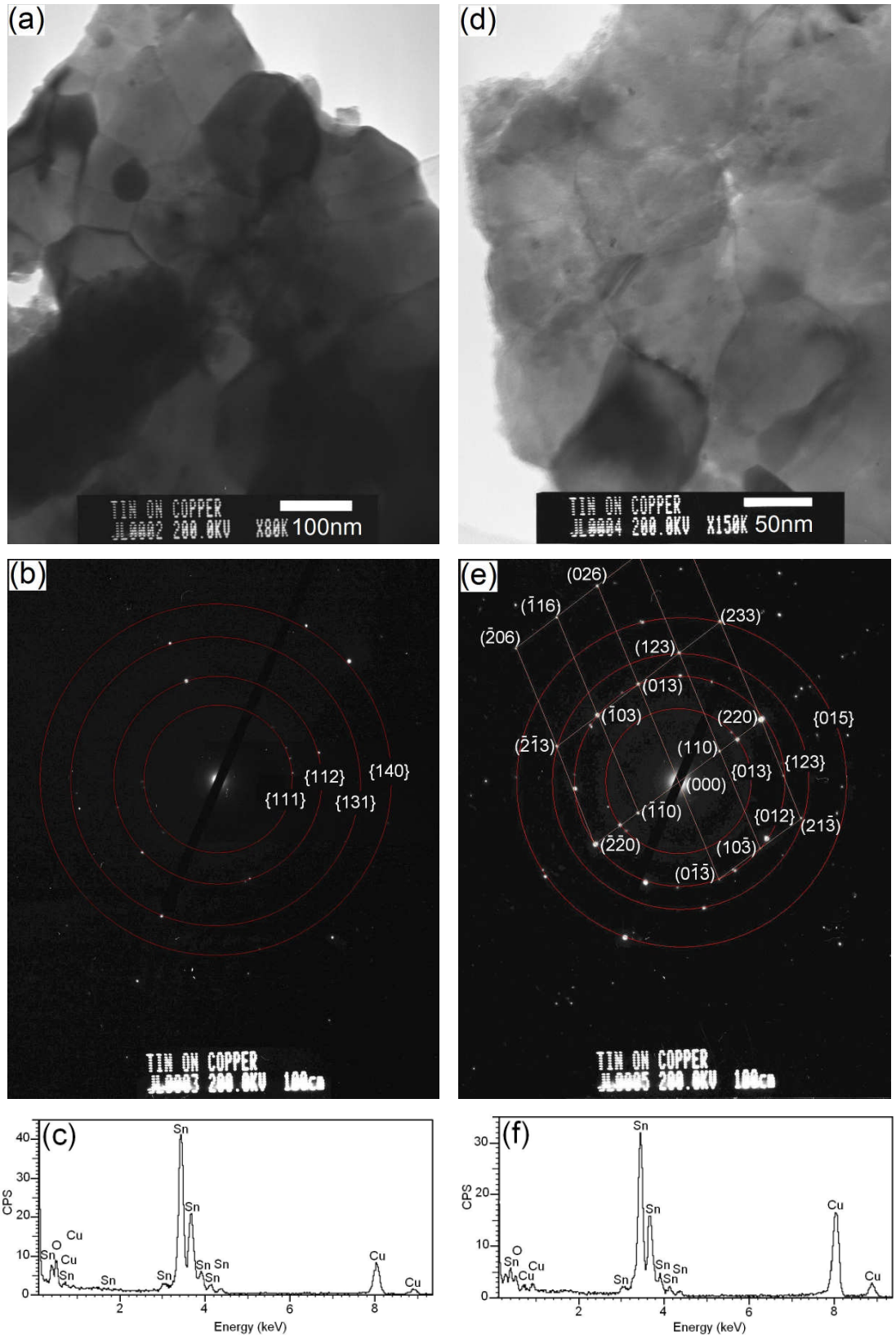

Fig. 8 TEM results of particles removed from the surface of coating AC1: (a) TEM image of one Sn particle; (b) selected area ED spots distributed along the diffraction rings drawn for SnO_2; (c) EDXS spectrum showing relatively higher O content around the selected area; (d) TEM image of another Sn particle; (e) selected area ED spots of zone $[\bar{3}3\bar{1}]$ or distributed along the diffraction rings drawn for Sn; and (f) EDXS spectrum showing low O content around this selected area.

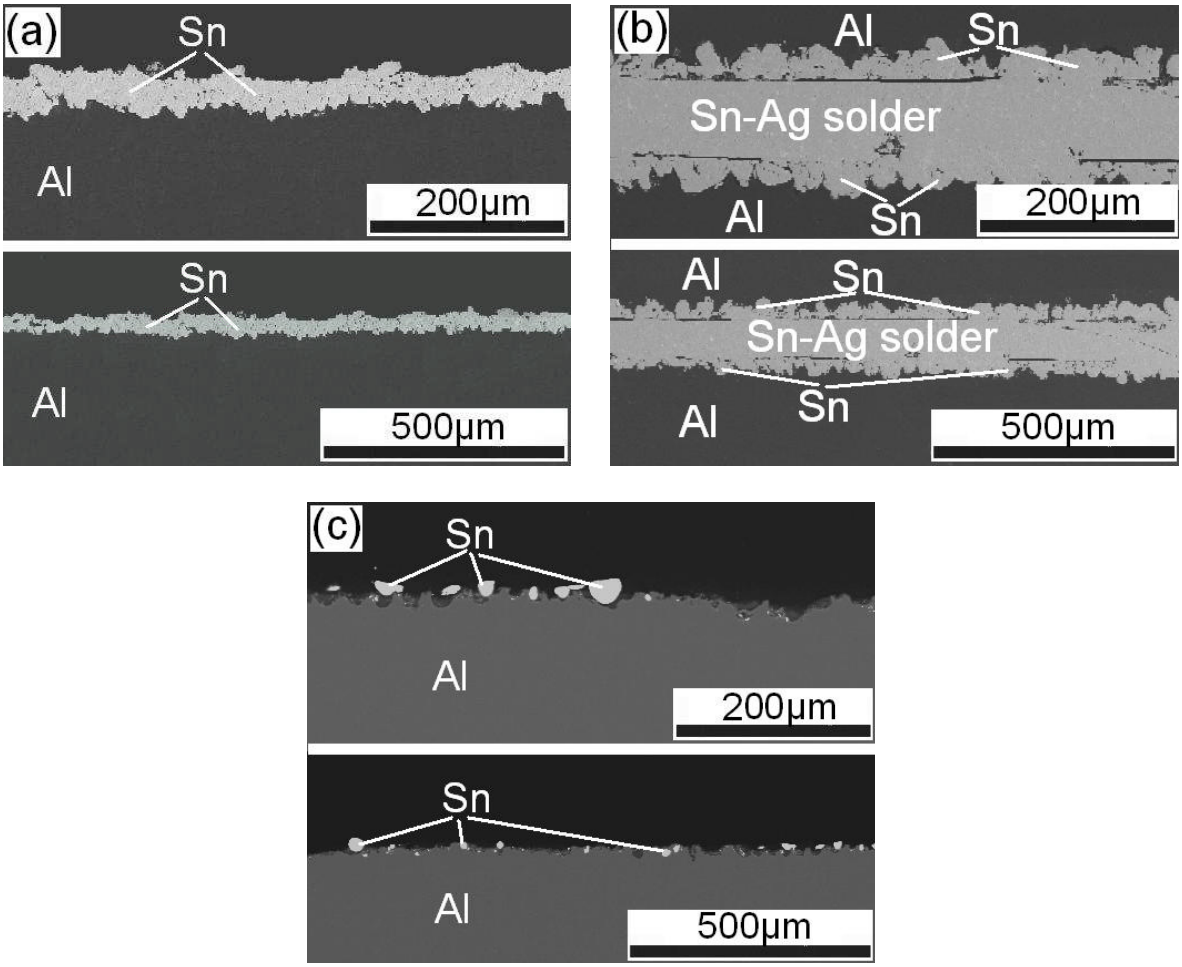

Fig. 9 SEM images of the polished cross sections of the Al/Sn-SnAg-Sn/Al (AA1) samples following different reflow processes: (a) RP1; (b) RP2; and (c) RP3.

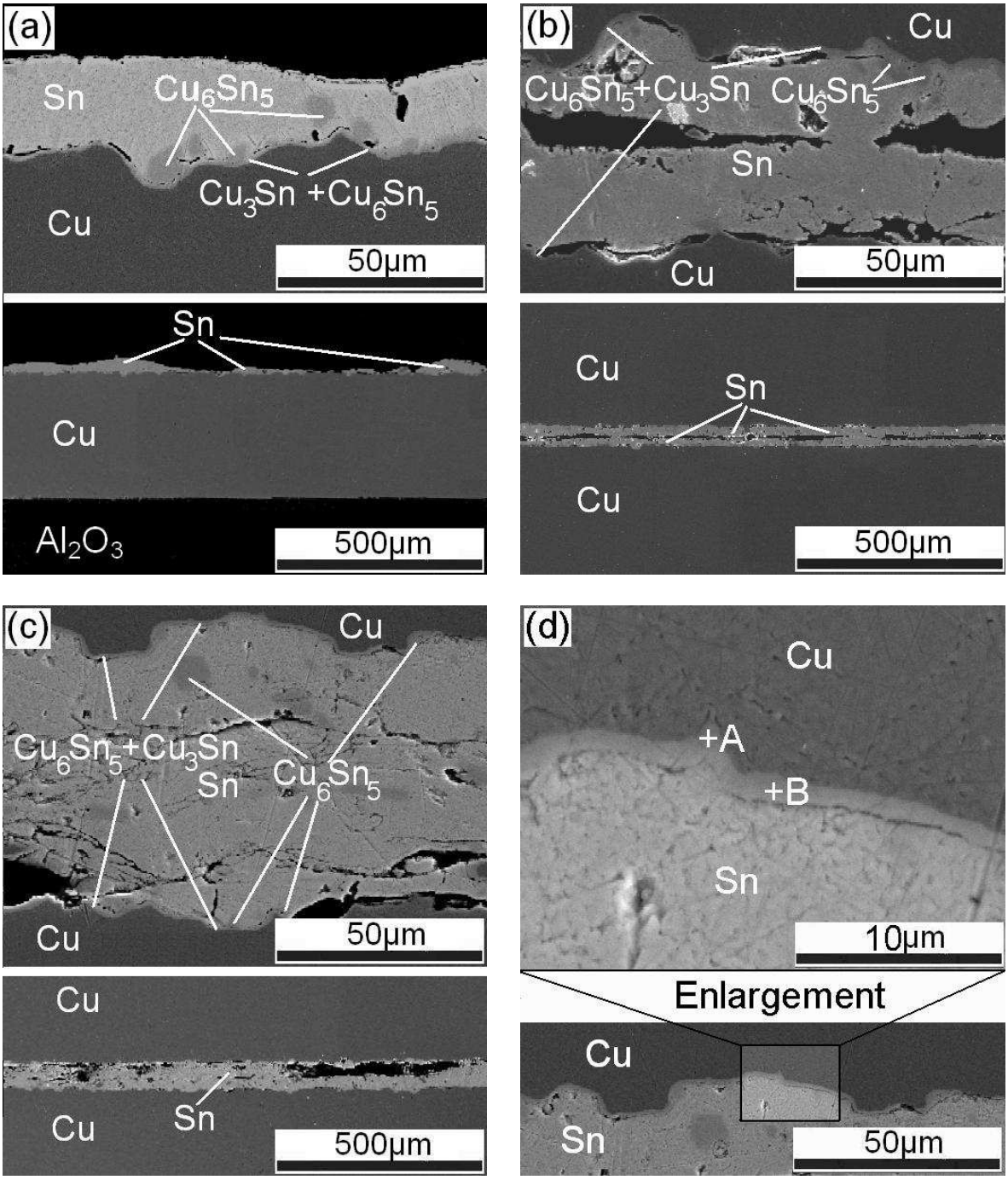

Fig. 10 SEM images of the polished cross sections of the DBC/Sn-Sn/DBC (AC1) samples following different reflow processes: (a) RP1; (b) RP2; (c) RP3, and (d) also RP3, enlarged view showing the morphology of intermetallic layer.